HHS Public Access

Author manuscript

Mol Cancer Ther. Author manuscript; available in PMC 2024 April 02.

Published in final edited form as:

Mol Cancer Ther. 2023 October 02; 22(10): 1215–1227. doi:10.1158/1535-7163.MCT-23-0210.

Intratumoral interleukin-15 improves efficacy of near-infrared photoimmunotherapy

Hiroshi Fukushima,

Aki Furusawa,

Takuya Kato,

Hiroaki Wakiyama,

Seiichiro Takao,

Shuhei Okuyama,

Peter L. Choyke,

Hisataka Kobayashi, M.D., Ph.D.

Molecular Imaging Branch, Center for Cancer Research, National Cancer Institute, NIH, Bethesda, MD, 20892, USA

Abstract

Interleukin (IL)-15 is a potent inducer of differentiation and proliferation of $CD8^+$ T and natural killer (NK) cells, making it a promising candidate for cancer immunotherapy. However, limited efficacy of systemic monotherapy utilizing intravenous IL-15 suggests needs for alternative routes of administration or combination treatment with other therapies. Near-infrared photoimmunotherapy (NIR-PIT) is a highly selective anti-cancer treatment that elicits massive release of tumor antigens and immunogenic signals. Here, we investigated whether intratumoral IL-15 can enhance the effectiveness of cancer cell-targeted NIR-PIT using syngeneic murine tumor models. Intratumoral injection of IL-15 was more effective than intraperitoneal IL-15 *in vivo* in suppressing tumor growth and inducing intratumoral immune responses. When the efficacy of CD44-targeted NIR-PIT was compared *in vivo* between IL-15-secreting MC38 (hIL-15-MC38) and parental MC38 tumors, the hIL-15-MC38/NIR-PIT group showed the best tumor growth inhibition and survival. Additionally, the hIL-15-MC38/NIR-PIT group showed significant dendritic cell maturation and significant increases in the number and Granzyme B expression of tumor-infiltrating $CD8^+$ T, NK, and natural killer T cells compared to the treated parental line. Furthermore, intratumoral IL-15 injection combined with CD44-targeted NIR-PIT showed significant tumor control in MC38 and Pan02-luc tumor models. In bilateral tumor models, CD44-targeted NIR-PIT in hIL-15-MC38 tumors significantly suppressed the growth of untreated MC38 tumors, suggesting abscopal effects. Mice that achieved complete response after the combination therapy completely rejected later tumor rechallenge. In conclusion, local IL-15 administration synergistically improves the efficacy of cancer cell-targeted NIR-PIT probably

Corresponding author: Hisataka Kobayashi, M.D., Ph.D., Molecular Imaging Branch, Center for Cancer Research, National Cancer Institute, NIH, 10 Center Drive, Bethesda, MD, 20892, USA, Tel: 240-858-3069; Fax: 240-541-4527; kobayash@mail.nih.gov.

Conflict of interest: The authors declare no potential conflicts of interest.

by inducing stronger anti-cancer immunity, indicating its potential as an anti-cancer treatment strategy.

Keywords

Cancer; Near-infrared photoimmunotherapy; Interleukin-15; T cell activation; Intratumoral immunotherapy

Introduction

Interleukin (IL)-15, a pleiotropic cytokine, is a potential therapeutic agent/adjuvant in the treatment of cancer as it stimulates host immune responses, including the differentiation and proliferation of $CD8^+$ T and natural killer (NK) cells (1,2). While IL-15 shares this function with IL-2, it does not cause activation-induced cell death of memory T cells or activation of regulatory T cells (Tregs), making it a more promising immunotherapy for the induction of potent anti-cancer immunity (3). However, human clinical trials have demonstrated that intravenous infusion of hIL-15 has modest efficacy but extensively expands peripheral NK cells, resulting in higher rates of severe dose-limiting toxicity (4). To overcome these limitations, studies have investigated the efficacy of various treatment strategies, including alternative routes of administration and the use of IL-15 in combination therapy (5–7). Local administration of IL-15 in the tumor can improve its delivery to the tumor microenvironment while reducing its systemic toxicity (8,9). Also, given that IL-15 monotherapy expands antigen-non-specific immunity (10), it would more effectively work when combined with other cancer-killing therapies that substantially release tumor antigens and activate anti-cancer acquired immunity.

Near-infrared photoimmunotherapy (NIR-PIT) is a novel anti-cancer treatment that utilizes an antibody-photoabsorber conjugate (APC) to bind the tumor whereupon subsequent NIR light exposure triggers selective photochemical reactions leading to immunogenic cell death (ICD) (11–13). The APC is constructed by conjugating the photoabsorber IRDye700DX (IR700) (11–13), a silica-phthalocyanine dye, to monoclonal antibodies directed against tumor antigens on the cancer cell membrane (11). NIR light irradiation provokes the dissociation of axial ligands within the IR700 molecule, converting it from highly hydrophilic to highly hydrophobic, causing aggregation of cell surface antigens-bound to the APCs (14). These photochemical reactions immediately damage the membrane of cancer cells, leading to swelling, blebbing, and rupture (14–16). NIR-PIT induces ICD by inducing the rapid release of immunogenic signals, such as calreticulin, ATP, HSP 70, and HSP 90, which activate immature dendritic cells (DCs) (17). Therefore, NIR-PIT is a potent anti-cancer therapy that not only directly kills cancer cells but also induces a potent anti-cancer immune response.

We hypothesized that local IL-15 administration could increase the effectiveness of cancer cell-targeted NIR-PIT by promoting the immune response. The CD44 protein, which is overexpressed on various cancer cells, serves as an attractive target for cancer therapy but is also useful in syngeneic mouse models because it is commonly expressed (18–21). This study aimed to investigate *in vivo* anti-cancer efficacy of local IL-15 administration

combined with CD44-targeted NIR-PIT in syngeneic murine cancer models, specifically using models of IL-15-auto-secretion and intratumoral IL-15 injection.

Materials and Methods

Synthesis of IR700-conjugated anti-CD44 monoclonal antibody

APC was synthesized as described previously (19). In brief, 1 mg of anti-mouse/human CD44 monoclonal antibody (6.7 nmol; clone IM7; Bio X Cell, West Lebanon, NH, USA) was incubated with five-fold molar excess of IR700 NHS ester (10 mM in DMSO; LI-COR Biosciences, Lincoln, NE, USA) in 100 mM Na_2HPO_4 solution (pH 8.5) for one hour at room temperature. The mixture was purified with PD-10 columns containing Sephadex G25 resin (GE Healthcare, Piscataway, NJ, USA). The resulting APC was abbreviated as CD44-IR700.

Cell culture

Murine cancer cell lines, MC38 (colon cancer) and Pan02-luc (pancreatic cancer), were used in this study. MC38 was kindly provided by Dr. Thomas Waldmann, NIH. Pan02-luc was purchased from GenTarget Inc (San Diego, CA, USA). Human IL-15-secreting MC38 (hIL-15-MC38) was constructed by introducing human IL-15-coding plasmids into MC38 cells as described previously (22,23). MC38 and Pan02-luc cells were cultured in RPMI1640 medium (Thermo Fisher Scientific, Rockford, IL, USA) supplemented with 10% FBS (Thermo Fisher Scientific) and 100 IU/mL penicillin/streptomycin (Thermo Fisher Scientific). hIL-15-MC38 cells were cultured in Dulbecco's Modified Eagle Medium (ATCC, Manassas, VA, USA) supplemented with 10% FBS and 100 IU/mL penicillin/streptomycin. All cells were cultured in a humidified incubator at 37 °C in an atmosphere of 95% air and 5% carbon dioxide. MC38 was authenticated by STR profiling (IDEXX BioAnalytics, Westbrook, ME, USA) in 2021. Pan02-luc was used in our laboratory within 6 months after receipt from the vendor. All cell lines were tested for Mycoplasma using PCR; MC38 was examined by IDEXX BioAnalytics in 2021 and hIL-15-MC38 and Pan02-luc were examined by Frederick National Laboratory for Cancer Research (Frederick, MD, USA) in 2022. Cells were frozen down soon after the authentication and Mycoplasma testing, and thawed to be used in this study. After thawing, cells were maintained in culture for no more than 30 passages

In vitro NIR-PIT

MC38 or hIL-15-MC38 cells were seeded at 1×10^5 onto 24-well plates in 1 mL of medium and incubated for 24 hours at 37 °C. Cells were incubated in culture medium containing CD44-IR700 (10 μg/mL) for 1 hour at 37 °C. After changing the medium into phenol-red-free medium, NIR laser-light (690 nm, 150 mW/cm^2) was applied using an ML7710 laser system (Modulight, Tampere, Finland). Cell-surface expression of calreticulin and HSP 70 was evaluated immediately after NIR light exposure. Cells were incubated for 30 minutes at 4 °C with anti-mouse calreticulin antibody (rabbit poly; Bioss Antibodies, Woburn, MA, USA) or its rabbit IgG1 isotype control (Bioss Antibodies) for calreticulin staining, and with anti-mouse/human HSP 70 antibody (clone REA349; Miltenyi Biotec, Gaithersburg, MD, USA) or its human IgG1 isotype control (clone REA293; Miltenyi Biotec) for HSP

70 staining. The fluorescence of cells was measured using BD FACSLyric (BD Biosciences, San Jose, CA, USA) and FlowJo software (FlowJo LLC, Ashland, OR, USA).

Animal models

All procedures were performed in compliance with the Guide for the Care and Use of Laboratory Animals and approved by the local Animal Care and Use Committee (MIP-003-4-L). Six- to eight-week-old female C57BL/6 (strain #000664) and homozygote athymic nude mice were purchased from the Jackson Laboratory (Bar Harbor, ME, USA). The lower part of the body of the mice was shaved before image analysis. Two million MC38, hIL-15-MC38, or Pan02-luc cells were inoculated into the right dorsum. Mice with tumors reaching approximately 50–150 mm^3 in volume were randomized for the experiments. For tumor rechallenge, 2×10^6 MC38 cells were inoculated into the left dorsum. For bilateral models, 1×10^6 MC38 and 2×10^6 hIL-15-MC38 cells were inoculated into the left and right sides of dorsal flank, respectively. Mice with a right tumor reaching approximately 30–50 mm^3 and a left tumor reaching approximately 50–150 mm^3 in volume were randomized for the experiment. Tumor volumes were defined as volume (mm^3) = length × $width^2$ × 0.5 and measured three times a week by a caliper. The mice were euthanized with CO_2 when the tumor reached 2 cm in diameter or 2,000 mm^3 in volume. For bilateral models, mice were euthanized when either tumor reached its endpoint. Alive mice were censored 60 days after NIR-PIT. Tumor disappearance for four weeks or longer after treatment was defined as complete remission (CR).

ELISA

One million MC38 or hIL-15-MC38 cells were incubated in 5 mL of medium at 37 °C for 72 hours; then supernatants were collected. MC38 or hIL-15-MC38 tumor-bearing mice were euthanized 14 days after inoculation. Tumors were harvested, and tumor homogenates were prepared. Peripheral blood samples were collected from mice, and plasma was prepared. Human IL-15 concentration was measured using Human IL-15 DuoSet ELISA kit (R&D Systems, Minneapolis, MN, USA) according to the manufacturer's protocol.

IL-15 administration

Human IL-15 (PeproTech, Rocky Hill, NJ, USA) was administered to mice intraperitoneally (5 μg in 100 μL PBS) or intratumorally (5 μg in 20 μL PBS) every other day four times in total.

In vivo NIR-PIT

To compare the efficacy of NIR-PIT among MC38 and hIL-15-MC38 tumors, mice were categorized into four groups as follows: (i) MC38 with no treatment (MC38/Control), (ii) MC38 treated with intravenous injection of CD44-IR700 (50 μg) followed by NIR light irradiation (MC38/NIR-PIT), (iii) hIL-15-MC38 with no treatment (hIL-15-MC38/Control), and (iv) hIL-15-MC38 treated with intravenous injection of CD44-IR700 (50 μg) followed by NIR light irradiation (hIL-15-MC38/NIR-PIT). To evaluate the efficacy of intratumoral IL-15 injection combined with NIR-PIT, mice were randomized into four groups as follows: (i) no treatment (Control), (ii) intravenous injection of CD44-IR700 (50 μg) followed

by NIR light irradiation (NIR-PIT), (iii) intratumoral IL-15 injection (IL-15-IT), and (iv) intravenous injection of CD44-IR700 (50 μg) followed by NIR light irradiation and intratumoral IL-15 injection (Combination). For bilateral tumor model experiments, mice were categorized into two groups as follows: (i) no treatment (Control) and (ii) intravenous injection of CD44-IR700 (50 μg) followed by NIR light irradiation (NIR-PIT). 690-nm NIR light (150 mW/cm^2, 50 J/cm^2, day 0) was administered to the tumors 24 hours after injecting CD44-IR700. When NIR light was applied, mice were covered by aluminum foil except for a hole to expose only the target tumor. In mice with CR after intratumoral IL-15 injection combined with NIR-PIT against MC38 tumors, 2×10^6 MC38 cells were re-inoculated into the contralateral dorsum 90 days after NIR-PIT. 700-nm fluorescence and white light images were obtained before and after NIR-PIT using a Pearl Imager (LI-COR Bioscience).

Flow cytometry

To compare tumor-infiltrating lymphocytes (TILs) between MC38 and hIL-15-MC38 tumors, we euthanized mice when established tumors reached approximately 150 mm^3 in volume. To assess the effect of intraperitoneal or intratumoral IL-15 injection on host tumor immunity, we harvested tumors one day after IL-15 injection. To assess host tumor immunity following CD44-targeted NIR-PIT, tumors and tumor draining lymph nodes (TDLNs) were harvested two and four days after NIR-PIT. Single-cell suspension was prepared as previously described (24,25). Cells were stained with the following antibodies: anti-CD3e (clone 145-2C11), anti-CD4 (clone RM4-5), anti-CD11b (clone M1/70), anti-CD11c (clone N418), anti-CD25 (clone PC61), anti-CD45 (clone 30-F11), anti-CD69 (clone H1.2F3), anti-CD83 (clone Michel-19), anti-CD86 (clone GL-1), anti-F4/80 (clone BM8), anti-Ki-67 (clone 10A8), anti-Ly6C (clone HK1.4), anti-I-A/I-E (clone M5/114.15.2), and anti-NK1.1 (clone PK136) were from BioLegend; anti-CD8α (clone 53-6.7), anti-CD45 (clone 30-F11), anti-Granzyme B (GZMB; clone NGZB), anti-FOXP3 (clone FJK-16s), anti-IL-15Rα (clone DNT15Ra), anti-Ly6G (clone 1A8), and rat IgG1 kappa isotype control (clone eBRG1) were from Thermo Fisher Scientific; anti-IL-15 (clone IC2471P) and mouse IgG1 isotype control (clone IC002P) were from R&D Systems. Dead cells were gated out by Fixable Viability Dye (Thermo Fisher Scientific). For membrane-bound IL-15 staining, single-cell suspension was incubated with human IL-15 (500 pM; PeproTech) for 15 minutes before antibody incubation. For intracellular staining of GZMB, cells were stimulated with eBioscience™ Cell Stimulation Cocktail plus protein transport inhibitors (Thermo Fisher Scientific) at 37 °C for four hours before staining. For intracellular and intranuclear staining, cells were fixed and permeabilized with Intracellular Fixation & Permeabilization Buffer Set (Thermo Fisher Scientific). The stained cells were analyzed using FACSLyric (BD Biosciences) and Flowjo software (FlowJo LLC). Cell types were determined as follows; $CD8^+$ T cells: $CD45^+/CD3^+/CD8^+/CD4^-$, $CD4^+$ T cells: $CD45^+/CD3^+/CD4^+/CD8^-$, Tregs: $CD45^+/CD3^+/CD4^+/CD8^-/FOXP3^+$, NK cells: $CD45^+/CD3^-/NK1.1^+$, natural killer T (NKT) cells: $CD45^+/CD3^+/NK1.1^+$, Myeloid cells: $CD45^+/CD11b^+$, DCs: $CD45^+/(F4/80)^-/CD11c^+/(I\text{-}A/I\text{-}E)^+$, Macrophages: $CD11b^+/(F4/80)^+$, and Monocytes: $CD11b^+/(F4/80)^-/Ly6G^-/Ly6C^+$. For IL-15 and IL-15Rα expression analyses, DCs were defined as $CD11b^-/(F4/80)^-/CD11c^+/(I\text{-}A/I\text{-}E)^+$.

Multiplex immunohistochemistry (IHC)

To analyze TIL distribution after CD44-targeted NIR-PIT, we harvested tumors four days after NIR-PIT, and formalin-fixed, paraffin-embedded sections were prepared. Multiplex IHC was performed as described previously, using Opal Automation IHC Kit (Akoya Bioscience, Menlo Park, CA, USA) and Bond RXm autostainer (Leica Biosystems, Wetzlar, Germany) (26,27). The sections were stained with 4,6-diamino-2-phenyl indole (DAPI) and the following antibodies: anti-CD3 (clone SP7; 1:500 dilution; Novus Biologicals, Littleton, CO, USA), anti-CD8 (clone EPR20305; 1:500 dilution; Abcam, Cambridge, MA, USA), anti-CD4 (clone EPR19514; 1:1000 dilution; Abcam), anti-FOXP3 (clone 1054C; 1:1000 dilution; Novus Biologicals), anti-pan-cytokeratin (pan-CK; rabbit poly; 1:250 dilution; Bioss Antibodies), anti-CD45 (clone D3F8Q; 1:500 dilution; Cell Signaling Technology, Danvers, MA, USA), anti-GZMB (rabbit poly; 1:500 dilution; Abcam), and anti-Ki-67 (clone D3B5; 1:500 dilution; Cell Signaling Technology). Coverslips were mounted using ProLong Diamond Antifade Mountant (Thermo Fisher Scientific). Stained slides were analyzed with Mantra Quantitative Pathology Workstation (Akoya Biosystems) and inForm Tissue Finder software (Akoya Biosystems). inForm software was trained to detect tissues and cell phenotypes according to the following criteria: areas with pan-CK expression = tumor, other areas = stroma, pan-$CK^+/CD8^-/CD4^-$ = cancer cells, pan-$CK^-/CD8^+/CD4^-$ = $CD8^+$ T cells, and pan-$CK^-/CD8^-/CD4^+$ = $CD4^+$ T cells, respectively. Four images were taken from each tumor sample, and cell density was calculated by combining areas for each tissue phenotype and cell counts of each cell phenotype. For GZMB expression analysis, cell phenotyping and GZMB expression analysis were performed separately for the same set of images, then cell segmentation data were consolidated and analyzed using phenoptrReports and phenoptr (Akoya Biosciences) to calculate the density of $GZMB^+CD8^+$ T cells. For Ki-67 expression analysis, cell phenotyping was performed as follows: pan-CK^+CD45^- = cancer cells, pan-CK^-CD45^+ = blood cells, and pan-CK^-CD45^- = other cells, respectively. The percentage of Ki-67 positive cells was computed among cancer cells. (See also Supplementary Table S1. List of key resource identifiers in this study)

Statistical analysis

Data are shown as mean ± SEM. GraphPad Prism 8.4.3 (GraphPad Software, La Jolla, CA, USA) was used for statistical analysis. A one-way ANOVA followed by Tukey's test was performed to compare data among multiple groups. Tumor volumes were compared using a repeated measures two-way ANOVA followed by Tukey's test. Survival percent was determined by a Kaplan-Meier method, and the results were compared using the log-rank test with Bonferroni correction. $P < 0.05$ was defined as statistically significant.

Data availability

The data generated in this study are available within the article and its Supplementary Data or from the corresponding author upon reasonable request.

Results

Intratumoral IL-15 injection elicited superior therapeutic efficacy and intratumoral immune responses to intraperitoneal injection

The therapeutic efficacy of local and systemic IL-15 administration was evaluated using *in vivo* tumor models. Mice with MC38 tumors reaching approximately 50–150 mm^3 in volume were divided into three groups: Control (untreated), IP (intraperitoneal IL-15 injection), and IT (intratumoral IL-15 injection). The IT group exhibited significantly slower tumor growth compared to the Control and IP groups (Fig. 1A). Additionally, the IT group exhibited the best survival among the three groups (Fig. 1B). Subsequently, intratumoral immune responses were assessed one day after a single dose treatment among the three groups (Fig. 1C and Supplementary Fig. S1). The IT group demonstrated a significant increase in the number of NK, myeloid, T, $CD8^+$ T, and NKT cells and DCs compared to the Control and IP groups (Fig. 1C and Supplementary Fig. S1A and S1B). Furthermore, GZMB expressions in $CD8^+$ T and NKT cells were significantly higher in the IT group compared to the Control and IP groups (Supplementary Fig. S1C). The number of Tregs was not significantly different among the three groups (Supplementary Fig. S1D).

Local IL-15 auto-secretion provided immunogenic tumor microenvironments and significant tumor control *in vivo*

Next, we evaluated the effects of local auto-secretion of IL-15 on *in vivo* tumor growth using hIL-15-MC38, an IL-15-secreting cell line. IL-15 auto-secretion was confirmed *in vitro* (Fig. 2A) and *in vivo* (Fig. 2B). However, there was no significant difference in plasma IL-15 levels between mice with hIL-15-MC38 and MC38 tumors (Fig. 2C). Based on chronological measurement of secreted IL-15, the amount of IL-15 secreted in a hIL-15-MC38 tumor was estimated to be approximately 1/50th of that in the intratumoral IL-15 injection (Supplementary Fig. S2). The growth of hIL-15-MC38 tumors was significantly slower than that of the parental MC38 tumors (Fig. 2D). Mice with hIL-15-MC38 tumors showed prolonged survival compared to those with MC38 tumors (Fig. 2E). However, hIL-15-MC38 tumors showed significantly higher Ki-67 positivity compared to MC38 tumors (Supplementary Fig. S3). Similar body weight trends were observed between mice with hIL-15-MC38 and MC38 tumors, suggesting an absence of acute toxicity in hIL-15-MC38 tumor-bearing mice (Fig. 2F).

We subsequently compared intratumoral immune cell profiles between hIL-15-MC38 and parental MC38 tumors (Fig. 2G and Supplementary Fig. S4). The number of NK, myeloid, T, $CD8^+$ T, and NKT cells was significantly higher in hIL-15-MC38 tumors than in MC38 tumors (Fig. 2G and Supplementary Fig. S4A). Although the number of Tregs was significantly higher in hIL-15-MC38 tumors compared to MC38 tumors, the proportion of Tregs was not significantly different between them (Supplementary Fig. S4B). IL-15Rα, an IL-15-specific receptor with a high affinity, mediates trans-presentation of IL-15, resulting in proliferation and activation of effector cells including NK and T cells. In both hIL-15-MC38 and MC38 tumors, IL-15Rα expression was slightly but significantly higher in monocytes compared to other immune cells (Fig. 2H). Similarly, a significantly higher level of membrane-bound IL-15 was detected in monocytes in comparison to other immune cells

(Fig. 2I). These results suggest that monocytes could be involved in IL-15 trans-presentation in the IL-15-auto-secretion model.

In vitro efficacy of CD44-targeted NIR-PIT against hIL-15-MC38 or MC38 cells

CD44 was highly expressed on the surface of hIL-15-MC38 and MC38 cells *in vitro* (Supplementary Fig. S5A). Flow-cytometric analysis confirmed the binding of CD44-IR700 to hIL-15-MC38 and MC38 cells *in vitro* (Supplementary Fig. S5B). Next, we examined the cytotoxic efficacy of *in vitro* CD44-targeted NIR-PIT against hIL-15-MC38 or MC38 cells. Microscopic examination showed that cellular swelling occurred in both cell lines immediately after NIR-PIT (Supplementary Fig. S5C). MTT assay showed a light-dose-dependent decrease in metabolic activity of hIL-15-MC38 and MC38 cells following NIR-PIT (Supplementary Fig. S5D and S5E). Furthermore, PI-positivity, an indicator of cell membrane damage, increased after NIR-PIT in a light-dose-dependent manner (Supplementary Fig. S5F and S5G). These results showed that CD44-targeted NIR-PIT induced cell death via cell membrane disruption in both hIL-15-MC38 and MC38 cells.

CD44-targeted NIR-PIT against hIL-15-MC38 tumors showed greater therapeutic efficacy *in vivo*

The therapeutic efficacy of *in vivo* CD44-targeted NIR-PIT was compared to that of the control using hIL-15-MC38 or parental MC38 tumor-bearing mice. The treatment and imaging schedule are shown in Figure 3A. Mice with tumors reaching approximately 50–150 mm^3 in volume were treated with or without NIR-PIT. NIR light was applied to tumors located on the right dorsal flank (Fig. 3B). Before NIR light irradiation, a 700-nm fluorescent signal was detected at the tumor site of mice in the NIR-PIT group due to the IR700 dye. After NIR light irradiation, this signal immediately decreased due to photoinduced bleaching of the conjugated IR700 (Fig. 3C). Among the four groups, the hIL-15-MC38/NIR-PIT group showed the slowest tumor growth (Fig. 3D). Furthermore, survival was significantly prolonged in the hIL-15-MC38/NIR-PIT group compared to the other groups (Fig. 3E). CR was achieved only in hIL-15-MC38/NIR-PIT group (2/11 mice, 18 %).

CD44-targeted NIR-PIT against hIL-15-MC38 tumors highly activated host immunity

We tested the expression of ICD-related molecules after *in vitro* CD44-targeted NIR-PIT against hIL-15-MC38 or parental MC38 cells. Calreticulin and HSP 70 expression significantly increased immediately after NIR-PIT in both cell lines, suggesting ICD (Fig. 4A; Fig. 4B; Supplementary Fig. S6).

Next, we evaluated host immune responses to CD44-targeted NIR-PIT in hIL-15-MC38 or parental MC38 tumors. In both tumors, the number of antigen-presenting cells including DCs, monocytes, and macrophages in tumors did not differ with or without NIR-PIT two days after NIR-PIT (Supplementary Fig. S7A). To evaluate DC maturation after NIR-PIT, the expression of DC maturation markers in tumor-draining lymph nodes (TDLNs) was analyzed by flow cytometry two days after NIR-PIT. CD83 and CD86 MFI in DCs significantly increased in the hIL-15-MC38/NIR-PIT group compared to the other three groups (Fig. 4C). In addition, $CD8^+$ T cell activation in TDLNs and tumors was

also assessed two days after NIR-PIT. In TDLNs, CD69 and CD25 were significantly upregulated, and Ki67 positivity was higher in the hIL-15-MC38/NIR-PIT group (Fig. 4D). In tumors, upregulation of CD69, but not CD25, was observed in the hIL-15-MC38/NIR-PIT group (Supplementary Fig. S7B). These results confirmed that $CD8^+$ T cells in TDLNs and tumors were highly activated and proliferating in the hIL-15-MC38/NIR-PIT group.

We further evaluated $CD8^+$ T cell infiltration and its cytotoxic potential in tumors by flow cytometry four days after NIR-PIT. The number of $CD8^+$ T cells was higher but equivalent in both the hIL-15-MC38/Control and hIL-15-MC38/NIR-PIT groups (Fig. 4E, *left*), regardless of NIR-PIT, suggesting that IL-15 primarily promoted the proliferation of $CD8^+$ T cells. GZMB expression in $CD8^+$ T cells was also significantly higher in the MC38/NIR-PIT and hIL-15-MC38/NIR-PIT groups (Fig. 4F, *left*), regardless of IL-15 secretion, indicating that NIR-PIT contributed to the enhanced cytotoxicity of $CD8^+$ T cells. The cytotoxic potential of NK and NKT cells was also analyzed by flow cytometry four days after NIR-PIT. The number of NK and NKT cells significantly increased in the hIL-15-MC38/Control and hIL-15-MC38/NIR-PIT groups (Fig. 4E, *middle and right*). GZMB expression in NK and NKT cells was significantly higher in the hIL-15-MC38/NIR-PIT group (Fig. 4F, *middle and right*).

Significant intratumoral infiltration of cytotoxic $CD8^+$ T cells after CD44-targeted NIR-PIT against hIL-15-MC38 tumors

In flow-cytometric analysis, the number of $CD8^+$ T cells was comparable between the hIL-15-MC38/Control and hIL-15-MC38/NIR-PIT groups. Given the disparity in *in vivo* efficacy between them, we hypothesized that NIR-PIT may primarily alter the distribution of $CD8^+$ T cells in tumors rather than their absolute number. Thus, we assessed TIL distribution after CD44-targeted NIR-PIT in hIL-15-MC38 or parental MC38 tumors. Tumors were harvested four days after each treatment and analyzed by multiplex IHC (Fig. 4G). $CD8^+$ T cell density in the tumor area was significantly higher in the hIL-15-MC38/NIR-PIT group than in the other three groups (Fig. 4H, *left*). GZMB expression in $CD8^+$ T cells was the highest in the hIL-15-MC38/NIR-PIT group (Fig. 4H, *right*). These findings were not present in the peritumoral stromal area (Fig. 4I). Additionally, we assessed Treg cell density and the ratio of $CD8^+$ T cells to Tregs, a well-known index of strong anti-cancer immunity (28). As shown in Supplementary Figure S8A and S8B, Treg cell density was comparable among the four groups in both the tumor and stroma areas. The hIL-15-MC38/NIR-PIT group showed higher $CD8^+$ T cells/Tregs ratio in the tumor area but not in the stromal area. Interestingly, a considerable number of $GZMB^+$ $CD8^-$ cells were observed in the hIL-15-MC38/NIR-PIT group (Supplementary Fig. S8C). These cells were a mixture of $CD3^-$ and $CD3^+$, suggestive of cytotoxic NK and NKT cells, respectively.

Intratumoral IL-15 injection combined with CD44-targeted NIR-PIT resulted in greater therapeutic efficacy and durable immunological memory

In vivo therapeutic efficacy of CD44-targeted NIR-PIT, intratumoral IL-15 injection, and the combination of the two was evaluated using mice with MC38 tumors reaching approximately 50–150 mm^3 in volume. Figure 5A illustrates the treatment regimen and schedule. Tumors in the right dorsal flank were irradiated with NIR light and/or injected

with IL-15 (Fig. 5B). A 700-nm fluorescent signal at the tumor site of mice was bleached immediately after NIR light irradiation in mice treated with NIR-PIT (Fig. 5C). Tumor growth was significantly slower in the Combination group than in the other three groups (Fig. 5D). Moreover, the Combination group showed the longest survival, and 55% of the mice achieved CR (Fig. 5E). In the IL-15-IT group, tumors were well controlled during IL-15 administration (Fig. 5D), but grew rapidly after IL-15 administration was completed. To evaluate the development of anti-cancer immunological memory, mice achieving CR were re-inoculated with MC38 cells approximately 13 weeks after the initial NIR-PIT on the contralateral dorsum (Fig. 5F). While allograft rejection was not observed in control mice, all the CR mice completely rejected the re-implanted MC38 cells (Fig. 5G and 5H). These results indicated that anti-cancer immunological memory was established after intratumoral IL-15 injection combined with CD44-targeted NIR-PIT.

Intratumoral IL-15 injection combined with CD44-targeted NIR-PIT was partially effective in T cell-deficient mice

To further evaluate the role of $CD8^+$ T cell immunity in the combination therapy, we tested the efficacy of intratumoral IL-15 injection combined with CD44-targeted NIR-PIT using athymic nude mice which lack T cells but have functional NK cells (Supplementary Fig. S9A–C). Tumor growth was significantly slower in the Combination group compared to the Control group (Supplementary Fig. S9D), but the combination therapy did not improve survival, and no mice achieved CR (Supplementary Fig. S9E). These results suggest that $CD8^+$ T cell immunity plays a pivotal role in anti-cancer immune responses in the setting of the combination therapy, albeit with a partial contribution from NK cells.

Intratumoral IL-15 injection combined with CD44-targeted NIR-PIT was highly effective against non-immunogenic pancreatic cancer

As intratumorally administered IL-15 binds to intratumoral immune cells, it is postulated that intratumoral IL-15 injection may be more efficacious in highly immunogenic tumors than in non-immunogenic tumors. However, our previous studies have demonstrated that CD44-targeted NIR-PIT can convert poorly immunogenic tumor microenvironments into highly immunogenic ones (21). Thus, we hypothesized that intratumoral IL-15 injection combined with CD44-targeted NIR-PIT might be effective against non-immunogenic pancreatic cancer models that are refractory to standard anti-cancer therapeutics (29). Accordingly, we used Pan02-luc tumors as a pancreatic cancer model. Multiplex IHC showed a lower density of TILs in Pan02-luc tumors compared to MC38 tumors (Supplementary Fig. S10). Pan02-luc cells highly expressed CD44, and CD44-targeted NIR-PIT was effective against them *in vitro* (Supplementary Fig. S11). Next, we compared the therapeutic efficacy of CD44-targeted NIR-PIT, intratumoral IL-15 injection, and their combination *in vivo* using mice with Pan02-luc tumors reaching approximately 50–150 mm^3 in volume. The treatment schedule is shown in Figure 6A. Confirmation of photobleaching at the tumor site via 700-nm fluorescent imaging was obtained upon exposure to NIR light (Fig. 6B). Tumor growth was significantly suppressed in the Combination group compared to the other three groups (Fig. 6C). Moreover, the Combination group showed significantly longer survival compared to the other three groups (Fig. 6D). However, none of the mice

in the Combination group attained CR; while some tumors temporarily disappeared after treatment they recurred in five of the ten mice (50%).

Local IL-15 administration combined with CD44-targeted NIR-PIT induced abscopal effects in distant untreated tumors

Finally, we assessed the development of systemic anti-cancer immunity using bilateral tumor models. To examine whether CD44-targeted NIR-PIT can induce abscopal effects, we treated only the right MC38 tumor, leaving the left MC38 tumor untreated, (Supplementary Fig. S12). The growth of the untreated tumors was similar between the Control and NIR-PIT groups, indicating that CD44-targeted NIR-PIT did not induce abscopal effects in distant untreated tumors.

Subsequently, we tested whether local IL-15 administration combined with CD44-targeted NIR-PIT showed anti-cancer effects in untreated tumors. Intratumoral IL-15 injection may leak into contralateral untreated tumors. Thus, we developed mice with hIL-15-MC38 tumors on the right dorsum and MC38 tumors on the left dorsum and administered NIR-PIT only to the right hIL-15-MC38 tumor (Fig. 7A and 7B). Immediately after NIR-PIT, a marked reduction in the 700-nm fluorescent signal was observed in the right tumor site, while the left tumor site remained unchanged (Fig. 7C). The NIR-PIT group exhibited a significant decrease in the growth of the treated tumors compared to the Control group (Fig. 7D). Notably, the untreated tumors in the NIR-PIT group also displayed a slower rate of growth when compared to the Control group (Fig. 7D). Additionally, the NIR-PIT group displayed a significantly prolonged survival rate in comparison to the Control group (Fig. 7E). We further analyzed TILs in the left untreated tumors four days after CD44-targeted NIR-PIT. The NIR-PIT group exhibited a significantly higher number of $CD8^+$ T, NK, and NKT cells compared to the Control group (Fig. 7F and Supplementary Fig. S13). Moreover, the NIR-PIT group showed significantly higher GZMB expression in $CD8^+$ T and NK cells compared to the Control group (Fig. 7G, *left* and *middle*). Although there was an increase in GZMB expression in NKT cells in the NIR-PIT group compared to the control group, this difference was not statistically significant (Fig. 7G, *right*). These results indicated that local IL-15 administration combined with CD44-targeted NIR-PIT elicited systemic anti-cancer immunity and abscopal effects in distant untreated tumors.

Discussion

In this study, we demonstrate that locally administrated IL-15, either injected intratumorally or produced by the cancer cells, exhibited synergistic therapeutic efficacy with CD44-targeted NIR-PIT in two mouse models. In both models, the combination therapy resulted in significantly slower tumor growth and prolonged survival compared to NIR-PIT alone. We confirmed that the combination therapy in the IL-15 auto-secretion model resulted in enhanced DC maturation and tumor infiltration of cytotoxic $CD8^+$, NK, and NKT cells. In mice that achieved CR after intratumoral IL-15 and NIR-PIT, subsequent tumor rechallenge was successful, indicating that immunological memory had been generated. Furthermore, the combination therapy induced abscopal effects in distant untreated tumors in bilateral tumor models in which only one tumor was treated. Therefore, local IL-15 administration is

an effective adjuvant to NIR-PIT, and its combination with cancer cell-targeted NIR-PIT can be utilized as an effective anti-cancer treatment strategy.

Previously we reported the efficacy of intraperitoneal IL-15 administration combined with CD44-targeted NIR-PIT using syngeneic murine cancer models (30). This combination therapy was effective, but it did not induce CR (30). In this study, the dose of CD44-IR700 was reduced to half of that in the previous study (30). Nevertheless, intratumoral IL-15 injection combined with NIR-PIT could achieve a higher CR rate in the MC38 tumor model. This suggests that intratumoral IL-15 administration is more efficacious as an anti-cancer immune booster when combined with NIR-PIT. By locally administering IL-15, a high concentration of IL-15 in the tumor microenvironment can directly stimulate intratumoral immune cells. Thus, NIR-PIT-activated cytotoxic $CD8^+$ T cells could be efficiently expanded by intratumorally administered IL-15.

Prior to combining it with NIR-PIT, we demonstrated that intratumoral injection of IL-15 was more effective than intraperitoneal injection in suppressing tumor growth and inducing intratumoral immune responses. In the two models we used, IL-15-auto-secretion and intratumoral IL-15 injection, it is difficult to directly compare efficacy. For instance, establishing accurate intratumoral IL-15 concentrations in the IL-15 auto-secretion model is challenging. We speculated that intratumoral IL-15 concentrations are likely lower in the IL-15-auto-secretion model than in the intratumoral IL-15 injection model (Supplementary Fig. S2). This may partially explain the variation in CR rates between the two models. Higher intratumoral IL-15 concentrations are crucial for therapeutic effectiveness. In IL-15-rich tumor microenvironments, IL-15Rα-expressing monocytes can more efficiently trans-present IL-15 to $CD8^+$ T and NK cells expressing IL-15Rβ/γC subunits (23,31). Additionally, a high concentration of IL-15 may modestly stimulate $CD8^+$ T and NK cells without IL-15 trans-presentation (1). Thus, augmenting intratumoral concentrations of IL-15 through molecular engineering may be a potential strategy for improving treatment success (9). Optimization of local administration methods, such as cancer-targeted vaccines and viruses that induce IL-15 secretion (9), may further improve this combination therapy.

We revealed significant efficacy of local IL-15 administration combined with CD44-targeted NIR-PIT in a Pan02-luc tumor model. Pancreatic cancer is well known to respond poorly to immunotherapy and is often refractory to many standard anti-cancer agents (32). Pan02-luc tumors share these features with clinical pancreatic cancer (29,33). Although no mice achieved CR after the combination therapy, tumors temporarily disappeared, and tumor growth was well controlled in 50% of the mice. This result suggests that local IL-15 administration combined with CD44-targeted NIR-PIT can treat non-immunogenic tumors by inducing an immune response.

This study has several limitations. First, human IL-15, but not murine IL-15, was used in this study. However, the utilization of human IL-15 in murine models is substantiated by multiple studies, wherein murine IL-15Rα trans-presented human IL-15 to murine CD8+ T cells, NK cells, and NKT cells, resulting in potent immunostimulatory effects that were comparable to those elicited by trans-presentation of murine IL-15 (34–36). Second, CD44-targeted NIR-PIT may deplete a subset of antigen-presenting cells because they express

CD44 (24). Because the number of intratumoral DCs, monocytes, and macrophages was not different between the hIL-15-MC38/Control and hIL-15-MC38/NIR-PIT groups two days after NIR-PIT, they would have been supplied from neighboring tissues and exposed to IL-15 immediately after NIR-PIT. NIR-PIT using targets that can selectively kill only cancer cells might provide even higher therapeutic efficacy. Third, the phenotype of hIL-15-MC38 cells is slightly different from that of MC38 cells. hIL-15-MC38 tumors had significantly higher Ki-67 positivity than MC38 tumors, implying that hIL-15-MC38 tumors were more biologically aggressive and exhibited more apoptosis. We speculate that this might be the result of cancer cells overcoming a more immunogenic tumor microenvironment. This phenotypic difference may explain the low CR rate after CD44-targeted NIR-PIT against hIL-15-MC38 tumors. Fourth, MC38 cells transfected with a control plasmid might have served as better control in this study. Fifth, orthotopic models, although technically difficult in our experiments, are more suitable for evaluating anti-cancer immunity induced by NIR-PIT (37). Finally, we did not determine the optimal therapeutic sequence of local IL-15 administration and NIR-PIT.

In conclusion, we demonstrate that local IL-15 administration combined with CD44-targeted NIR-PIT yielded synergistic anti-cancer immunity, resulting in eradication of the treated tumor, abscopal effects in distant untreated tumors, and establishment of immunologic memory. While technological advancements in local IL-15 administration are necessary to efficiently administer IL-15 and achieve higher intratumoral concentrations, our findings provide a rationale for exploring the therapeutic potential of local IL-15 administration combined with cancer cell-targeted NIR-PIT in a clinical trial setting.

Supplementary Material

Refer to Web version on PubMed Central for supplementary material.

Financial support:

This work was supported by the Intramural Research Program of the National Institutes of Health, National Cancer Institute, Center for Cancer Research (award recipient: Hisataka Kobayashi, grant number: ZIA BC 011513).

References

1. Fiore PF, Di Matteo S, Tumino N, Mariotti FR, Pietra G, Ottonello S, et al. Interleukin-15 and cancer: some solved and many unsolved questions. J Immunother Cancer 2020;8:e001428 [PubMed: 33203664]
2. Waldmann TA, Miljkovic MD, Conlon KC. Interleukin-15 (dys)regulation of lymphoid homeostasis: Implications for therapy of autoimmunity and cancer. J Exp Med 2020;217:e20191062 [PubMed: 31821442]
3. Berger C, Berger M, Hackman RC, Gough M, Elliott C, Jensen MC, et al. Safety and immunologic effects of IL-15 administration in nonhuman primates. Blood 2009;114:2417–26 [PubMed: 19605850]
4. Conlon KC, Lugli E, Welles HC, Rosenberg SA, Fojo AT, Morris JC, et al. Redistribution, hyperproliferation, activation of natural killer cells and CD8 T cells, and cytokine production during first-in-human clinical trial of recombinant human interleukin-15 in patients with cancer. J Clin Oncol 2015;33:74–82 [PubMed: 25403209]

5. Chen W, Bamford RN, Edmondson EF, Waldmann TA. IL15 and Anti-PD-1 Augment the Efficacy of Agonistic Intratumoral Anti-CD40 in a Mouse Model with Multiple TRAMP-C2 Tumors. Clin Cancer Res 2022;28:2082–93 [PubMed: 35262675]
6. Hangasky JA, Chen W, Dubois SP, Daenthanasanmak A, Muller JR, Reid R, et al. A very long-acting IL-15: implications for the immunotherapy of cancer. J Immunother Cancer 2022;10:e004104 [PubMed: 35101947]
7. Nelson A, Gebremeskel S, Lichty BD, Johnston B. Natural killer T cell immunotherapy combined with IL-15-expressing oncolytic virotherapy and PD-1 blockade mediates pancreatic tumor regression. J Immunother Cancer 2022;10:e003923 [PubMed: 35246474]
8. Baniel CC, Sumiec EG, Hank JA, Bates AM, Erbe AK, Pieper AA, et al. Intratumoral injection reduces toxicity and antibody-mediated neutralization of immunocytokine in a mouse melanoma model. J Immunother Cancer 2020;8:e001262 [PubMed: 33115944]
9. Melero I, Castanon E, Alvarez M, Champiat S, Marabelle A. Intratumoural administration and tumour tissue targeting of cancer immunotherapies. Nat Rev Clin Oncol 2021;18:558–76 [PubMed: 34006998]
10. Alves NL, Hooibrink B, Arosa FA, van Lier RA. IL-15 induces antigen-independent expansion and differentiation of human naive CD8+ T cells in vitro. Blood 2003;102:2541–6 [PubMed: 12805064]
11. Kobayashi H, Choyke PL. Near-Infrared Photoimmunotherapy of Cancer. Acc Chem Res 2019;52:2332–9 [PubMed: 31335117]
12. Mitsunaga M, Ogawa M, Kosaka N, Rosenblum LT, Choyke PL, Kobayashi H. Cancer cell-selective in vivo near infrared photoimmunotherapy targeting specific membrane molecules. Nat Med 2011;17:1685–91 [PubMed: 22057348]
13. Fukushima H, Turkbey B, Pinto PA, Furusawa A, Choyke PL, Kobayashi H. Near-Infrared Photoimmunotherapy (NIR-PIT) in Urologic Cancers. Cancers (Basel) 2022;14:2996 [PubMed: 35740662]
14. Sato K, Ando K, Okuyama S, Moriguchi S, Ogura T, Totoki S, et al. Photoinduced Ligand Release from a Silicon Phthalocyanine Dye Conjugated with Monoclonal Antibodies: A Mechanism of Cancer Cell Cytotoxicity after Near-Infrared Photoimmunotherapy. ACS Cent Sci 2018;4:1559–69 [PubMed: 30555909]
15. Ogata F, Nagaya T, Okuyama S, Maruoka Y, Choyke PL, Yamauchi T, et al. Dynamic changes in the cell membrane on three dimensional low coherent quantitative phase microscopy (3D LC-QPM) after treatment with the near infrared photoimmunotherapy. Oncotarget 2017;8:104295–302 [PubMed: 29262641]
16. Nagaya T, Friedman J, Maruoka Y, Ogata F, Okuyama S, Clavijo PE, et al. Host Immunity Following Near-Infrared Photoimmunotherapy Is Enhanced with PD-1 Checkpoint Blockade to Eradicate Established Antigenic Tumors. Cancer Immunol Res 2019;7:401–13 [PubMed: 30683733]
17. Ogawa M, Tomita Y, Nakamura Y, Lee MJ, Lee S, Tomita S, et al. Immunogenic cancer cell death selectively induced by near infrared photoimmunotherapy initiates host tumor immunity. Oncotarget 2017;8:10425–36 [PubMed: 28060726]
18. Chen C, Zhao S, Karnad A, Freeman JW. The biology and role of CD44 in cancer progression: therapeutic implications. J Hematol Oncol 2018;11:64 [PubMed: 29747682]
19. Nagaya T, Nakamura Y, Okuyama S, Ogata F, Maruoka Y, Choyke PL, et al. Syngeneic Mouse Models of Oral Cancer Are Effectively Targeted by Anti-CD44-Based NIR-PIT. Mol Cancer Res 2017;15:1667–77 [PubMed: 28923838]
20. Maruoka Y, Furusawa A, Okada R, Inagaki F, Fujimura D, Wakiyama H, et al. Near-Infrared Photoimmunotherapy Combined with CTLA4 Checkpoint Blockade in Syngeneic Mouse Cancer Models. Vaccines (Basel) 2020;8:528 [PubMed: 32937841]
21. Wakiyama H, Furusawa A, Okada R, Inagaki F, Kato T, Maruoka Y, et al. Increased Immunogenicity of a Minimally Immunogenic Tumor after Cancer-Targeting Near Infrared Photoimmunotherapy. Cancers (Basel) 2020;12:3747 [PubMed: 33322807]

22. Bamford RN, DeFilippis AP, Azimi N, Kurys G, Waldmann TA. The 5' untranslated region, signal peptide, and the coding sequence of the carboxyl terminus of IL-15 participate in its multifaceted translational control. J Immunol 1998;160:4418–26 [PubMed: 9574546]
23. Kobayashi H, Dubois S, Sato N, Sabzevari H, Sakai Y, Waldmann TA, et al. Role of trans-cellular IL-15 presentation in the activation of NK cell-mediated killing, which leads to enhanced tumor immunosurveillance. Blood 2005;105:721–7 [PubMed: 15367431]
24. Furusawa A, Okada R, Inagaki F, Wakiyama H, Kato T, Furumoto H, et al. CD29 targeted near-infrared photoimmunotherapy (NIR-PIT) in the treatment of a pigmented melanoma model. Oncoimmunology 2022;11:2019922 [PubMed: 35003897]
25. Kato T, Fukushima H, Furusawa A, Okada R, Wakiyama H, Furumoto H, et al. Selective depletion of polymorphonuclear myeloid derived suppressor cells in tumor beds with near infrared photoimmunotherapy enhances host immune response. Oncoimmunology 2022;11:2152248 [PubMed: 36465486]
26. Fukushima H, Kato T, Furusawa A, Okada R, Wakiyama H, Furumoto H, et al. Intercellular adhesion molecule-1-targeted near-infrared photoimmunotherapy of triple-negative breast cancer. Cancer Sci 2022;113:3180–92 [PubMed: 35723065]
27. Kato T, Okada R, Furusawa A, Inagaki F, Wakiyama H, Furumoto H, et al. Simultaneously Combined Cancer Cell- and CTLA4-Targeted NIR-PIT Causes a Synergistic Treatment Effect in Syngeneic Mouse Models. Mol Cancer Ther 2021;20:2262–73 [PubMed: 34518299]
28. Quezada SA, Peggs KS, Curran MA, Allison JP. CTLA4 blockade and GM-CSF combination immunotherapy alters the intratumor balance of effector and regulatory T cells. J Clin Invest 2006;116:1935–45 [PubMed: 16778987]
29. Priebe TS, Atkinson EN, Pan BF, Nelson JA. Intrinsic resistance to anticancer agents in the murine pancreatic adenocarcinoma PANC02. Cancer Chemother Pharmacol 1992;29:485–9 [PubMed: 1348974]
30. Maruoka Y, Furusawa A, Okada R, Inagaki F, Wakiyama H, Kato T, et al. Interleukin-15 after Near-Infrared Photoimmunotherapy (NIR-PIT) Enhances T Cell Response against Syngeneic Mouse Tumors. Cancers (Basel) 2020;12:2575 [PubMed: 32927646]
31. Dubois S, Mariner J, Waldmann TA, Tagaya Y. IL-15Ralpha recycles and presents IL-15 In trans to neighboring cells. Immunity 2002;17:537–47 [PubMed: 12433361]
32. Lutz ER, Wu AA, Bigelow E, Sharma R, Mo G, Soares K, et al. Immunotherapy converts nonimmunogenic pancreatic tumors into immunogenic foci of immune regulation. Cancer Immunol Res 2014;2:616–31 [PubMed: 24942756]
33. Putzer BM, Rodicker F, Hitt MM, Stiewe T, Esche H. Improved treatment of pancreatic cancer by IL-12 and B7.1 costimulation: antitumor efficacy and immunoregulation in a nonimmunogenic tumor model. Mol Ther 2002;5:405–12 [PubMed: 11945067]
34. Stoklasek TA, Schluns KS, Lefrancois L. Combined IL-15/IL-15Ralpha immunotherapy maximizes IL-15 activity in vivo. J Immunol 2006;177:6072–80 [PubMed: 17056533]
35. Eisenman J, Ahdieh M, Beers C, Brasel K, Kennedy MK, Le T, et al. Interleukin-15 interactions with interleukin-15 receptor complexes: characterization and species specificity. Cytokine 2002;20:121–9 [PubMed: 12453470]
36. Kim PS, Kwilas AR, Xu W, Alter S, Jeng EK, Wong HC, et al. IL-15 superagonist/IL-15RalphaSushi-Fc fusion complex (IL-15SA/IL-15RalphaSu-Fc; ALT-803) markedly enhances specific subpopulations of NK and memory CD8+ T cells, and mediates potent anti-tumor activity against murine breast and colon carcinomas. Oncotarget 2016;7:16130–45 [PubMed: 26910920]
37. Hoffman RM. Orthotopic metastatic mouse models for anticancer drug discovery and evaluation: a bridge to the clinic. Invest New Drugs 1999;17:343–59 [PubMed: 10759402]

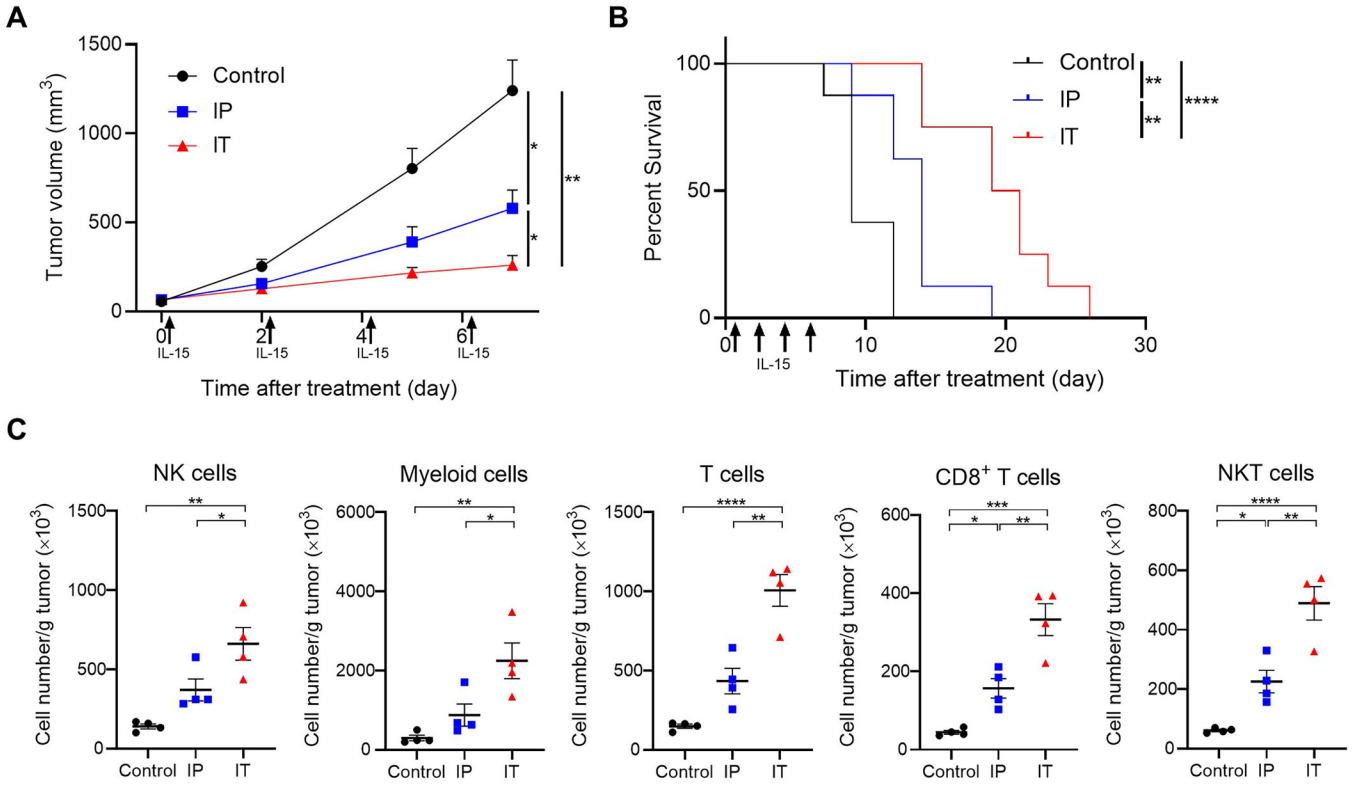

Figure 1.

In vivo therapeutic efficacy of intratumoral injection of human IL-15 in a MC38 tumor mouse model. A, Tumor growth curves after IL-15 treatment. Mice with MC38 tumors reaching approximatey 50–150 mm^3 in volume were used. Human IL-15 (5 μg) was intraperitoneally (IP) or intratumorally (IT) administered to mice (day 0, 2, 4, and 6) and tumor growth was compared among the three groups showing slower growth in IL-15-exposed tumors ($n = 7$; mean ± SEM; repeated measures two-way ANOVA followed by Tukey's test); *, $p < 0.05$; **, $p < 0.01$. B, Survival curves after IL-15 treatment (n = 7, log–rank test with Bonferroni correction); **, $p < 0.01$; ****, $p < 0.0001$. C, Host immune responses after IL-15 treatment. A single dose (5 μg) of IL-15 were intraperitoneally or intratumorally administered to MC38 tumor-bearing mice. One day after IL-15 treatment, the tumors were harvested and analyzed by flow cytometry demonstrating increased number of immune cells in tumors treated with IL-15 IT (n = 4; mean ± SEM; one-way ANOVA followed by Tukey's test); *, $p < 0.05$; **, $p < 0.01$; ***, $p < 0.001$; ****, $p < 0.0001$.

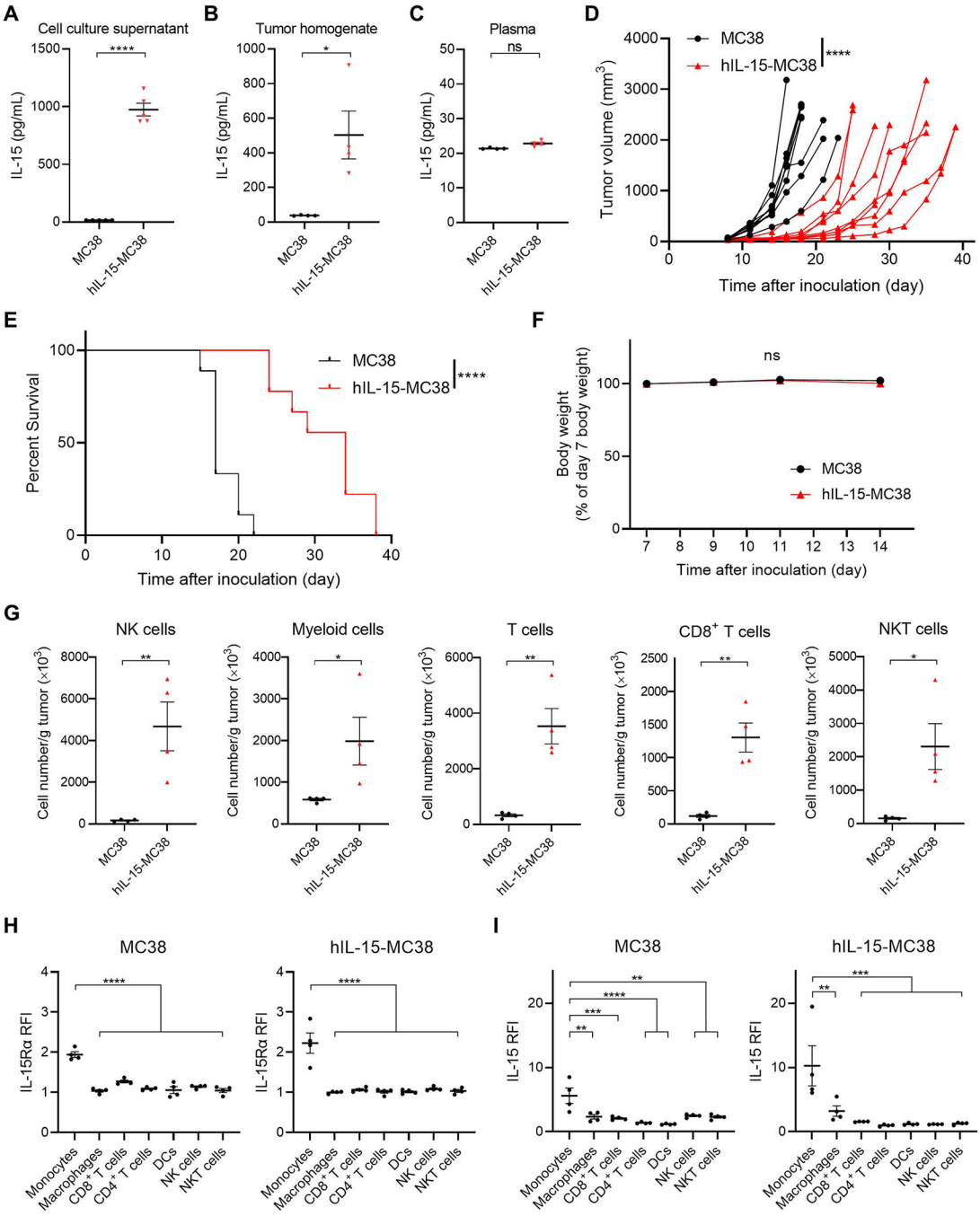

Figure 2.

Characterization of hIL-15-MC38 cells in comparison with parental MC38 cells. A, IL-15 concentrations in cell culture supernatant after 72 h incubation of hIL-15-MC38 or parental MC38 cells (n = 4; mean ± SEM; unpaired t test); ****, $p < 0.0001$. B, IL-15 concentrations in homogenates of hIL-15-MC38 or parental MC38 tumors (n = 4; mean ± SEM; unpaired t test); *, $p < 0.05$. Tumors were harvested and tumor homogenates were prepared 14 days after inoculation. C, IL-15 concentrations in serum samples of hIL-15-MC38 or MC38 tumor-bearing mice (n = 4; mean ± SEM; unpaired t test); ns, not significant. Peripheral

blood samples were collected and plasma was prepared 14 days after inoculation. D, Growth curves of hIL-15-MC38 or parental MC38 tumors showing delayed growth (n = 9; mean ± SEM; repeated measures two-way ANOVA followed by Sidak's test); ****, $p < 0.0001$. E, Survival curves of hIL-15-MC38 or MC38 tumor-bearing mice showing improved survival (n = 9, log–rank test); ****, $p < 0.0001$. F. Changes in body weight of hIL-15-MC38 or MC38 tumor-bearing mice were minimal. Body weight measurement started seven days after tumor inoculation (n = 5; mean ± SEM; repeated measures two-way ANOVA followed by Sidak's test); ns, not significant. G, Immune cell expressions in hIL-15-MC38 tumors. hIL-15-MC38 or MC38 tumors were harvested and analyzed by flow cytometry demonstrating significant increase in most immune cell subsets (n = 4; mean ± SEM; unpaired t test); *, $p < 0.05$; **, $p < 0.01$. H, IL-15Rα expression in the tumor microenvironments of hIL-15-MC38 or MC38 tumors. hIL-15-MC38 or MC38 tumors were harvested and analyzed by flow cytometry (n = 4; mean ± SEM; one-way ANOVA followed by Tukey's test); ****, $p < 0.0001$ vs. monocytes; RFI, relative fluorescence intensity. I, Detection of membrane-bound IL-15 in immune cells of hIL-15-MC38 or MC38 tumors. hIL-15-MC38 or MC38 tumors were harvested and dissociated into single cell suspensions. They were incubated with human IL-15 (500 pM) for 15 minutes and analyzed by flow cytometry (n = 4; mean ± SEM; one-way ANOVA followed by Tukey's test); **, $p < 0.01$; ***, $p < 0.001$; ****, $p < 0.0001$ vs. monocytes.

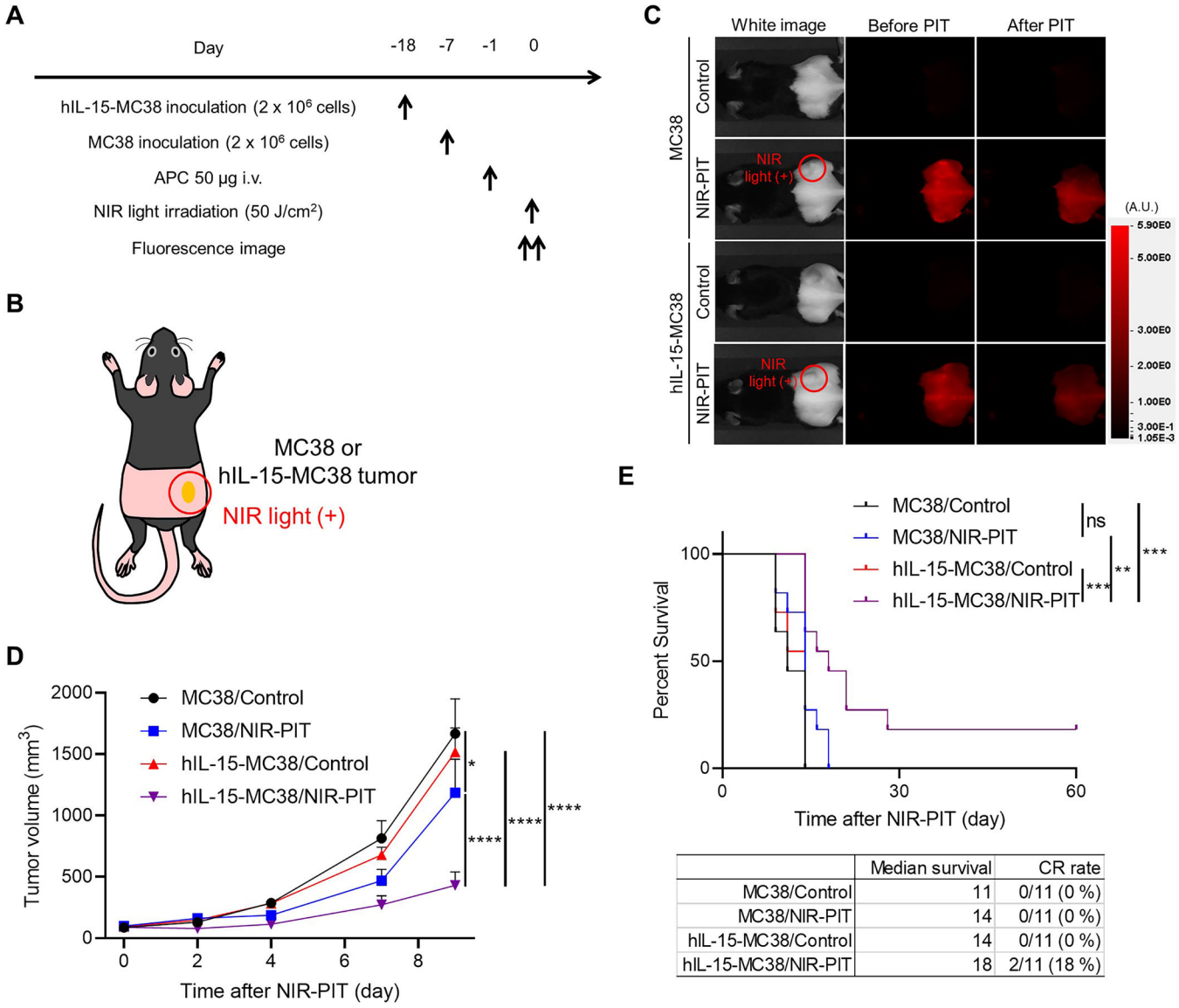

	Median survival	CR rate
MC38/Control	11	0/11 (0 %)
MC38/NIR-PIT	14	0/11 (0 %)
hIL-15-MC38/Control	14	0/11 (0 %)
hIL-15-MC38/NIR-PIT	18	2/11 (18 %)

Figure 3.

In vivo therapeutic efficacy of CD44-targeted NIR-PIT in a hIL-15-MC38 vs. parental MC38 tumor mouse model. A, Treatment schedule. Mice with hIL-15-MC38 or MC38 tumors reaching approximately 50–150 mm^3 in volume were treated with or without NIR-PIT. B, Diagram of NIR light irradiation. The red circle represents where NIR light was irradiated. C, Representative fluorescent imaging at 700 nm before and after NIR-PIT in hIL-15-MC38 or MC38 tumor-bearing mice. A.U., arbitrary units. D, Tumor growth curves showing delayed growth in hIL-15 MC38 cells after NIR-PIT vs. controls (n = 11; mean ± SEM; repeated measures two-way ANOVA followed by Tukey's test); *, $p < 0.05$; ****, $p < 0.0001$. E, Survival curves shows enhanced survival in hIL-15 MC38 tumors treated with NIR-PIT (n = 11, log–rank test with Bonferroni correction); **, $p < 0.01$; ***, $p < 0.001$; ns, not significant; CR, complete response.

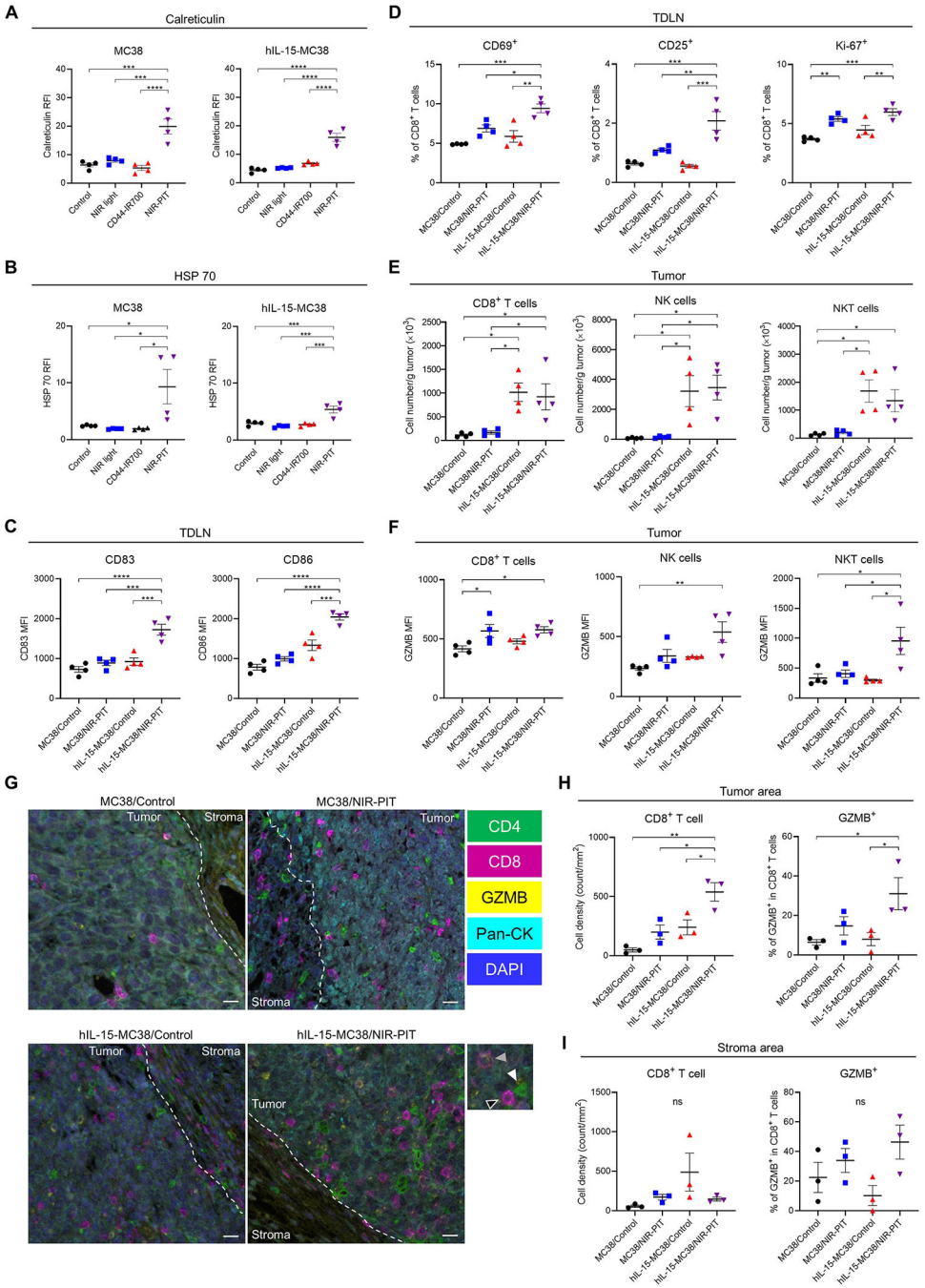

Figure 4.

Host immune responses after CD44-targeted NIR-PIT against hIL-15-MC38 tumors. A and B, Expression of immunogenic signals immediately after *in vitro* CD44-targeted NIR-PIT in hIL-15-MC38 or parental MC38 cells. Calreticulin (A) and heat shock protein (HSP) 70 are increased (B) immediately after *in vitro* CD44-targeted NIR-PIT ($n = 4$; mean ± SEM; one-way ANOVA followed by Tukey's test); ***, $p < 0.001$; ****, $p < 0.0001$; RFI, relative fluorescence intensity. C and D, Immune cell populations in tumor draining lymph nodes (TDLNs) of hIL-15-MC38 or MC38 models were evaluated by flow cytometry two days

after CD44-targeted NIR-PIT. CD83 (C, *left*) and CD86 (C, *right*) expressions in dendritic cells (DCs) and CD69 (D, *left*), CD25 (D, *middle*), and Ki-67 (D, *right*) expressions in $CD8^+$ T cells in the TDLNs (n = 4; mean ± SEM; one-way ANOVA followed by Tukey's test); *, $p < 0.05$; **, $p < 0.01$; ***, $p < 0.001$; ****, $p < 0.0001$; ns, not significant; MFI, mean fluorescence intensity. E and F, Immune cell populations in hIL-15-MC38 or MC38 tumors were evaluated by flow cytometry four days after CD44-targeted NIR-PIT. The cell number/g tumor (E) and Granzyme B (GZMB) expression (F) for $CD8^+$ T, NK, and NKT cells in tumors (n = 4; mean ± SEM; one-way ANOVA followed by Tukey's test); *, $p < 0.05$; **, $p < 0.01$. G-I, Immune cell distributions in hIL-15-MC38 or MC38 tumors were evaluated by multiplex immunohistochemistry (IHC) four days after CD44-targeted NIR-PIT. G, Representative pictures (images; ×200; scale bar, 20 μm). Staining of CD4, CD8, GZMB, and pan-cytokeratin (pan-CK) are shown in green, magenta, yellow, and cyan, respectively. Nucleus is stained with DAPI and shown in blue. Tumor area is shown in white dotted line. The inset shows examples of $CD4^+$ T cell (white-filled arrowhead), $CD8^+$ T cell (open arrowhead), and $GZMB^+CD8^+$ T cell (gray-filled arrowhead). H, $CD8^+$ T cell density (*left*) and GZMB expression in $CD8^+$ T cells (*right*) in the tumor area (n = 3; mean ± SEM; one-way ANOVA followed with Tukey's test); *, $p < 0.05$; **, $p < 0.01$. I, $CD8^+$ T cell density (*left*) and GZMB expression in $CD8^+$ T cells (*right*) in the stroma area (n = 3; mean ± SEM; one-way ANOVA followed with Tukey's test); ns, not significant.

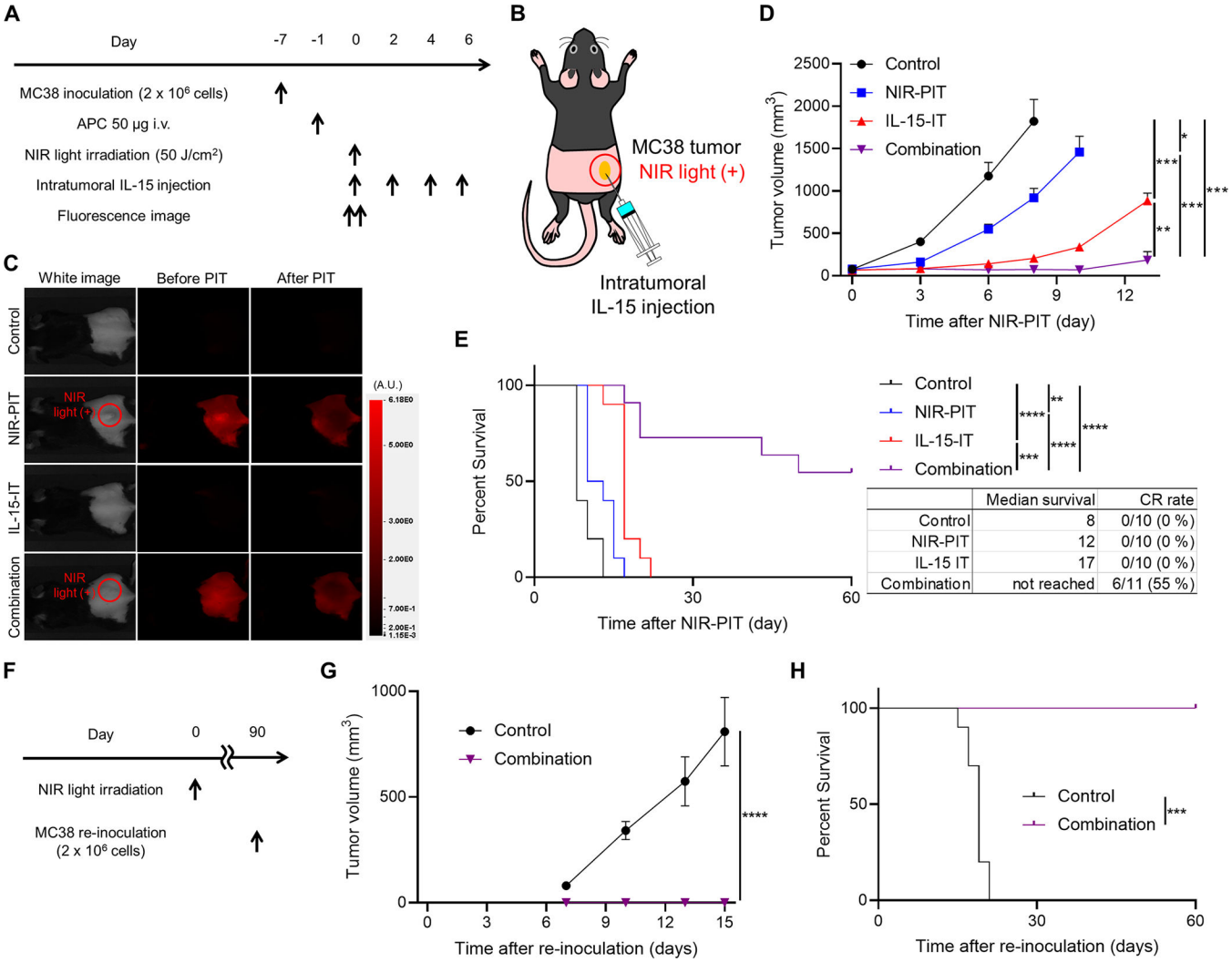

Figure 5.

Intratumoral IL-15 injection combined with CD44-targeted NIR-PIT significantly suppressed tumor growth, prolonged survival, and induced anti-cancer immunological memory *in vivo* in a MC38 tumor mouse model compared to controls with no therapy or only one of the therapies. A, Treatment schedule. Mice with MC38 tumors reaching approximately 50–150 mm^3 in volume were treated with CD44-targeted NIR-PIT, intratumoral IL-15 injection, or their combination. B, Diagram of NIR light irradiation. The red circle represents where NIR light was irradiated. C, Representative fluorescent imaging at 700 nm before and after NIR-PIT. A.U., arbitrary units. D, Tumor growth curves (n = 10–11; mean ± SEM; repeated measures two-way ANOVA followed by Tukey's test); *, $p < 0.05$; **, $p < 0.01$; ***, $p < 0.001$. E, Survival curves (n = 10–11, log–rank test with Bonferroni correction); **, $p < 0.01$; ***, $p < 0.001$; ****, $p < 0.0001$; CR, complete response. F, Schedule of MC38 tumor rechallenge. G, Tumor growth curves after MC38 tumor rechallenge showing no growth in tumors previously treated successfully by the combination (n = 6; mean ± SEM; repeated measures two-way ANOVA followed by Sidak's test); ****, $p < 0.0001$. H, Survival curves after MC38 tumor rechallenge show

complete survival in mice that underwent combination therapy and achieved a CR previously indicating the development of long-term immune memory against this tumor strain (n = 6, log–rank test); ***, $p < 0.001$.

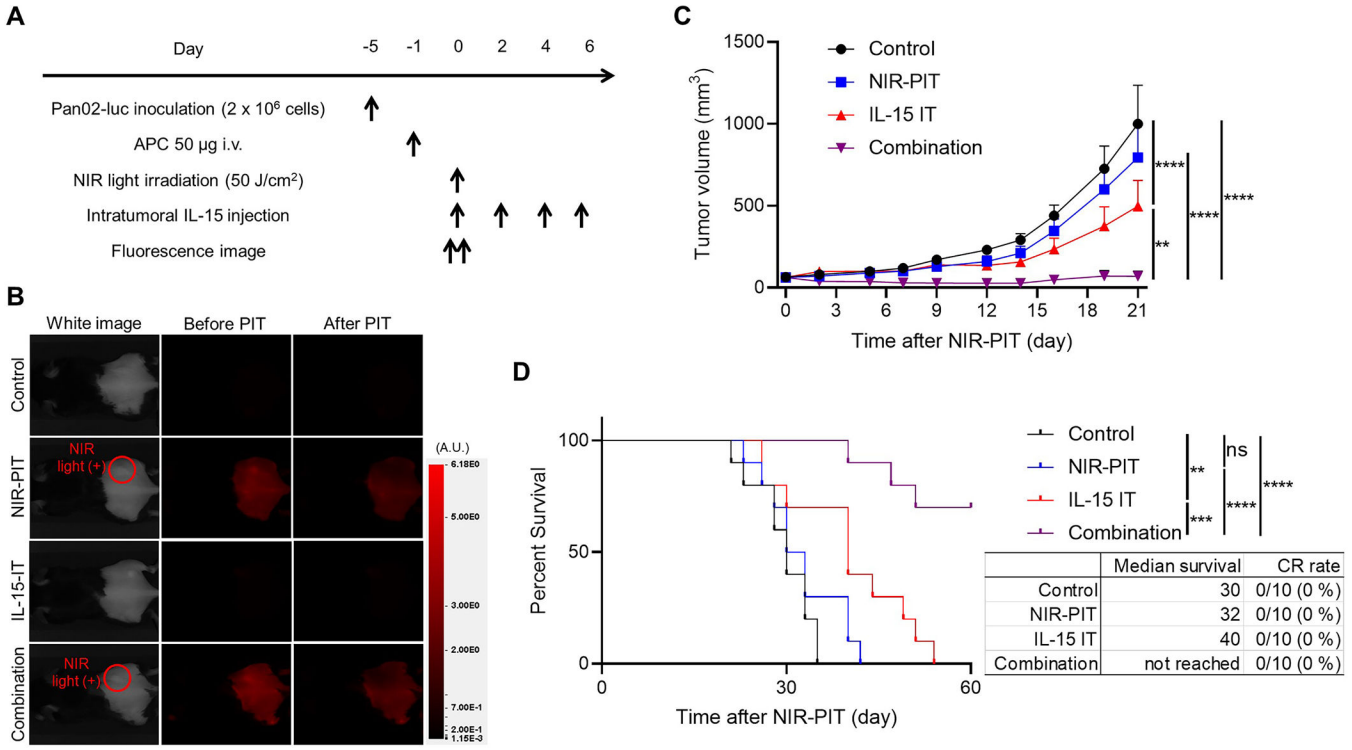

Figure 6.

In vivo therapeutic efficacy of intratumoral IL-15 injection combined with CD44-targeted NIR-PIT in a Pan02-luc tumor mouse model, which is known not to be non-immunogenic. A, Treatment schedule. Mice with Pan02-luc tumors reaching approximately 50–150 mm^3 in volume were treated with CD44-targeted NIR-PIT, intratumoral IL-15 injection, or their combination. B, Representative fluorescent imaging at 700 nm before and after NIR-PIT. A.U., arbitrary units. C, Tumor growth curves showing effectiveness of combination therapy (n = 10; mean ± SEM; repeated measures two-way ANOVA followed by Tukey's test); **, $p < 0.01$; ****, $p < 0.0001$. D, Survival curves showing prolonged surviving in mice receiving combination therapy although no CRs were achieved in this group (n = 10, log–rank test with Bonferroni correction); **, $p < 0.01$; ***, $p < 0.001$; ****, $p < 0.0001$; CR, complete response.

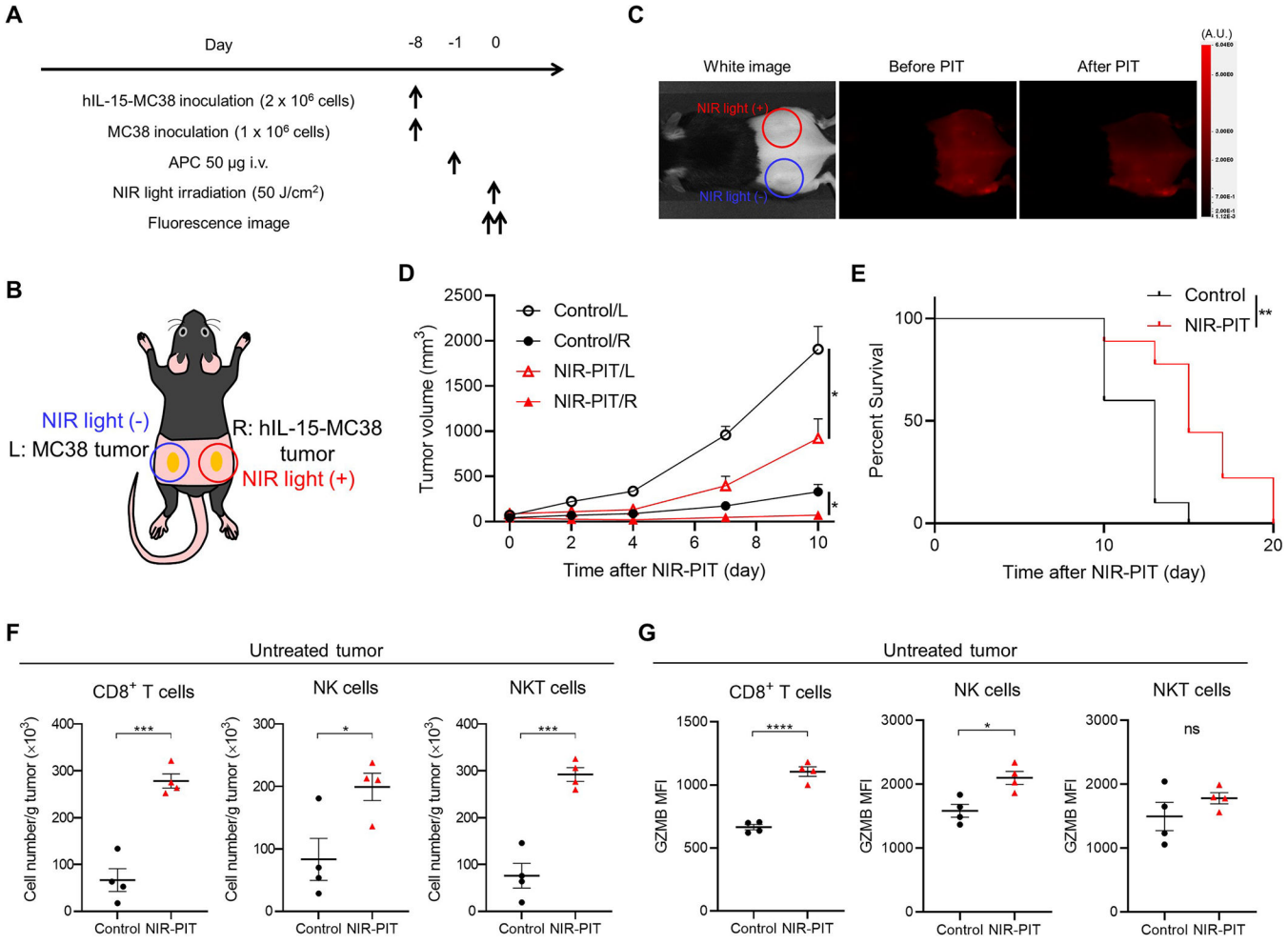

Figure 7.

In vivo therapeutic efficacy of CD44-targeted NIR-PIT in a bilateral tumor mouse model (R: hIL-15-MC38 tumor, L: MC38 tumor). NIR light was irradiated only to the right tumor. The left tumor was not exposed to NIR light. A, Treatment schedule. B, Diagram of NIR light irradiation. The red circle represents where NIR light was irradiated. C, Representative fluorescent imaging at 700 nm before and after NIR-PIT. A.U., arbitrary units. D, Tumor growth curves demonstrating partial abscopal effect in the untreated left tumor (n = 9–10; mean ± SEM; repeated measures two-way ANOVA followed by Tukey's test); *, $p < 0.05$. E, Survival curves (n = 9–10, log–rank test); **, $p < 0.01$. F and G, Immune cell populations in untreated left tumors were evaluated by flow cytometry four days after CD44-targeted NIR-PIT demonstrating immune cell infiltration. The cell number/g tumor (F) and Granzyme B (GZMB) expression (G) for $CD8^+$ T cells, NK cells, and NKT cells in untreated left tumors (n = 4; mean ± SEM; one-way ANOVA followed by Tukey's test); *, $p < 0.05$; ***, $p < 0.001$; ****, $p < 0.0001$; ns, not significant.